This article has been accepted for inclusion in a future issue of this journal. Content is final as presented, with the exception of pagination.

Spectrum-Time Estimation and Processing (STEP) for Improving Weather Radar Data Quality

Qing Cao, *Member, IEEE*, Guifu Zhang, *Senior Member, IEEE*, Robert D. Palmer, Michael Knight, Ryan May, and Robert J. Stafford

***Abstract*—This paper introduces the Spectrum-Time Estimation and Processing (STEP) algorithm developed in the Atmospheric Radar Research Center (ARRC) at the University of Oklahoma (OU). The STEP processing framework integrates three novel algorithms recently developed in ARRC: spectrum clutter identification, bi-Gaussian clutter filtering, and multi-lag moment estimation. The three modules of STEP algorithm fulfill three functions: clutter identification, clutter filtering and noise reduction, respectively. The performance of STEP has been evaluated using simulated data as well as real data collected by the C-band polarimetric research radar OU-Polarimetric Radar for Innovations in Meteorology and Engineering. Results show that STEP algorithm can effectively improve quality of polarimetric weather data in the presence of ground clutter and noise.**

***Index Terms*—Meteorological radar, parameter estimation, radar clutter, radar detection, radar signal processing.**

I. Introduction

WEATHER radar has become an indispensable tool for modern weather services around the world. The quality of radar data is essential to the performance of various meteorological applications such as severe weather detection, precipitation estimation, and weather forecasting. Ground clutter and noise, however, are two major factors that adversely affect the quality of radar data. Ground clutter, which is normally present in the radar observations at a low elevation and/or in the near range, heavily biases the weather measurements such as power, mean velocity, spectrum width, and polarimetric parameters. Noise, another main source of error, limits the radar sensitivity from weak weather echoes and causes measurement biases as well. The removal of ground clutter and noise effect would lead to the more accurate measurement of weather phenomena and consequently improve radar's performance in meteorological applications.

Ground clutter is attributed to radar signal returns from ground targets such as trees, buildings, towers, mountains, etc. Generally speaking, ground targets are stationary or only have slow motions. Therefore, the Doppler spectrum of ground clutter is mainly located around zero Doppler velocity. Traditional clutter filtering methods apply a time-domain notch filter, suppressing the ground clutter as well as any weather signal around zero velocity [1]. Recently, clutter filtering in the frequency domain has become popular. For example, Siggia and Passarelli [2] proposed the well-known Gaussian Model Adaptive Processing (GMAP) method, which can recover the weather spectrum after notching the spectrum around zero velocity. The use of phased array techniques also helps the clutter filtering [3]. With advances in clutter filtering, it was realized that the filtering could bias the weather signal and should not be applied at all times, particularly for radar signals without clutter contamination but having a small Doppler velocity. Hence, clutter identification has attracted much research interest. One of the most recent identification algorithms is the Clutter Mitigation Decision (CMD) method proposed by Hubbert *et al.* [4]. CMD is based on the characteristic feature of several integral parameters (e.g., clutter phase alignment, CPA). Also, Warde and Torres [5] introduced the CLutter Environment ANalysis using Adaptive Processing, which utilized the phase of lag-one auto-correlation spectral density. Moisseev and Chandrasekar [6] identified the clutter contamination using the method of spectrum decomposition. The latter two algorithms apply the spectrum information, including both spectrum phase and spectrum amplitude. Recently, Li *et al.* [7] proposed a novel spectrum clutter identification (SCI) algorithm. This algorithm introduces two new spectrum parameters, spectral power discriminant (SPD) and spectral phase fluctuation (SPF), as well as two texture parameters, power texture (PT), and spectrum width texture (SWT). Li *et al.* have demonstrated that SCI has a better performance than CMD, particularly for regions with low clutter-to-signal-ratio (CSR) and those with very small Doppler velocity.

Conventional moment estimation methods use only one or two lags of the autocorrelation function (ACF) and/or cross-correlation function (CCF) to estimate various moments [8]. For example, signal power is estimated from the zero lag of ACF, and spectrum width is estimated with lags zero and one. Since the noise positively biases the zero lag of ACF, the estimates of signal power and spectrum width are enlarged, and signal correlation between polarimetric channels is reduced. When signal-to-noise ratio (SNR) is lower, the noise effect tends to be more serious. Some efforts have been made to improve the estimation under the low SNR condition [9]–[11]. Melnikov and Zrnić [9] suggested using the lag one estimator to substitute the lag zero estimator as a method to reduce the noise effect. Zhang *et al.* [10] proposed to exclude the zero

Manuscript received September 8, 2011; revised January 31, 2012; accepted February 26, 2012. This work was supported in part by the National Science Foundation under Grant AGS-1046171 and EEC project "Spectrum-Time Estimation and Processing (STEP) for Weather Radar Signals."

Q. Cao is with the Atmospheric Radar Research Center, The University of Oklahoma, Norman, OK 73072-7307 USA (e-mail: qingcao@ou.edu).

G. Zhang and R. D. Palmer are with the Atmospheric Radar Research Center, The University of Oklahoma, Norman, OK 73072-7307 USA and also with the School of Meteorology, The University of Oklahoma, Norman, OK 73072-7307 USA (e-mail: guzhang1@ou.edu; rpalmer@ou.edu).

M. Knight, R. May, and R. Stafford are with the Enterprise Electronics Corporation (EEC), Enterprise, AL 36330 USA (e-mail: mike.knight@eecradar.com; ryan.may@eecradar.com; bob.stafford@eecradar.com).

Color versions of one or more of the figures in this paper are available online at http://ieeexplore.ieee.org.

Digital Object Identifier 10.1109/TGRS.2012.2190608

0196-2892/$31.00 © 2012 IEEE

This article has been accepted for inclusion in a future issue of this journal. Content is final as presented, with the exception of pagination.

lag and use other lags (multiple lags) to improve correlation and wind estimations. Recently, the multilag estimator has been extended for enhancing polarimetric radar data [12], [13]. Cao *et al.* [14], [15] modified this multi-lag method with an adaptive-weight fitting. The multi-lag method optimizes the use of different lags and reduces the noise effect on the moment estimation.

In cooperation with Enterprise Electronics Corporation (EEC), the Atmospheric Radar Research Center (ARRC) at the University of Oklahoma (OU) has developed a Spectrum-Time Estimation and Processing (STEP) algorithm, aiming to improve the quality of polarimetric radar data in the presence of ground clutter and noise. This algorithm has been tested using the C-band polarimetric research radar OU-Polarimetric Radar for Innovations in Meteorology and Engineering (PRIME) [16]) and will be implemented soon in EEC's operational radar platform. The STEP algorithm integrates three novel algorithms recently developed in ARRC, including the aforementioned SCI algorithm [7] and multi-lag moment estimator (MLAG) [12]–[15]. The third algorithm is the bi-Gaussian clutter filtering method (BGCF), which fits the clutter-contaminated weather spectrum with a bi-Gaussian model. Accordingly, STEP consists of three major modules or steps: SCI, BGCF, and MLAG, that fulfill three functions: clutter identification, clutter filtering, and moment estimation, respectively. This paper intends to give an overall introduction of the STEP algorithm and demonstrate its performance using simulated and real data. Technical details of the three modules are not the emphasis of this paper, and their concepts will only be briefly addressed. More technical details of the SCI and MLAG algorithms can be obtained from previous studies [7], [12]–[15].

This paper is organized as follows: the STEP algorithm, including SCI, BGCF, and MLAG modules, is introduced in Section II; the performance evaluation of each module is given in Section III; a case study of STEP is shown in Sections IV and V provides the conclusions.

II. Description of the Step Algorithm

A. Overview

The STEP algorithm includes three major modules or steps, as shown in the flowchart in Fig. 1. First, the I/Q data (radar level-1 data) from the horizontal (H) and vertical (V) polarization channels are input into the SCI module (step 1). This module makes the decision on the identification of clutter contamination. If clutter contamination is determined, the BGCF module (step 2) will remove the ground clutter in the spectral domain and reconstruct the I/Q data using the filtered spectrum for the moment estimation in MLAG module (step 3). A complementary function is included in the BGCF module. When the BGCF method has a slow convergence, or fails to converge, a single-Gaussian clutter filtering method, similar to the concept of GMAP, is applied. If there is no clutter contamination, the original I/Q data are conveyed directly to the MLAG module (step 3) to estimate polarimetric parameters.

B. Spectrum Clutter Identification (SCI)

Recently, Li *et al.* [7] have proposed the SCI algorithm, which uses a fuzzy-logic classification framework with four

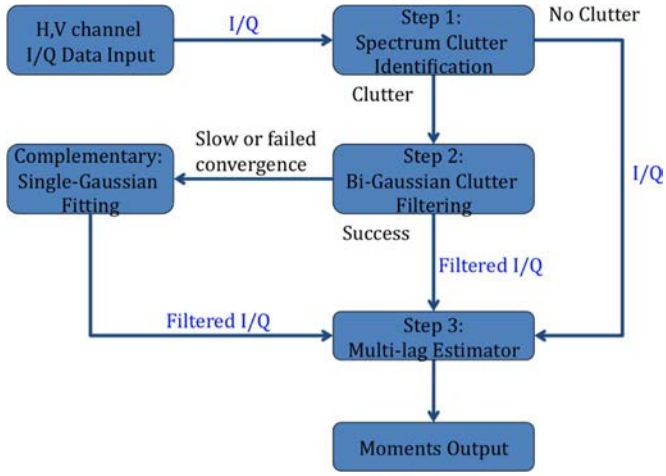

Fig. 1. Flowchart of STEP algorithm.

characteristic inputs, i.e., SPD, SPF, PT, and SWT. This algorithm is designed for single-polarization radar data. The details of SCI algorithm can be found in [7], and their results have shown better probability of detection (POD) and probability of false alarm (PFA) than CMD algorithm, particularly for radar echoes with low CSRs and/or small Doppler velocity. The SCI algorithm used in STEP algorithm adds an option for operation on polarimetric radars. In such a case, the correlation coefficient ($\rho_{\rm hv}$) is applied as an additional input to the SCI algorithm. As we know, the $\rho_{\rm hv}$ value for ground clutter is generally lower than the $\rho_{\rm hv}$ value for precipitation, meaning that $\rho_{\rm hv}$ can help with the identification of ground clutter [17], [18]. For example, the hydrometeor classification algorithm (HCA) developed by Park *et al.* [18] applies a $\rho_{\rm hv}$ range of 0.5–0.95 in the membership function to identify ground clutter. The SCI module in STEP applies a similar membership function to the HCA, with only a minor change. For a $\rho_{\rm hv}$ value from 0.5 to 0.8, the output of the membership function is 1; for a $\rho_{\rm hv}$ value from 0.8 to 0.95, the output changes linearly from 1 to 0; for a $\rho_{\rm hv}$ value beyond the range of 0.5–0.95; the output is 0. Accordingly, the final defuzzification equation in [7] changes to

$$\frac{(f_{SPD}+f_{SPF}+2\max[f_{PT},f_{SWT}]+f_{\rho_{hv}})}{5} \underset{H_0}{\overset{H_1}{\gtrless}} 0.5 \quad (1)$$

where, $f_{\rm SPD}$, $f_{\rm SPF}$, $f_{\rm PT}$, $f_{\rm SWT}$, and $f_{\rho \rm hv}$ are aggregation values for five parameters, respectively, in this fuzzy logic scheme. Five aggregation values, which are evaluated using their membership functions, represent the contribution of each measurement and indicate how likely they connect with the output identification. The criterion H_1 works for the detection of clutter and requires the left side value to be greater than 0.5. Otherwise, it will be identified as no clutter contamination, according to criteria H_0.

C. Bi-Gaussian Clutter Filtering (BGCF)

The BGCF algorithm removes ground clutter in the spectral domain. The fundamental assumption of BGCF is that both weather signal and ground clutter have a power spectrum of Gaussian shape, which has also been assumed in [19]. The

This article has been accepted for inclusion in a future issue of this journal. Content is final as presented, with the exception of pagination.

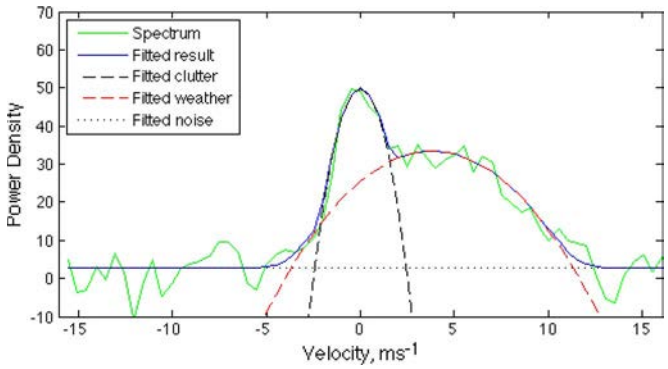

Fig. 2. Example of bi-Gaussian clutter filtering.

total power spectrum of the radar signal consists of three components: ground clutter, weather signal, and noise. It is modeled by

$$S(v) = s_c \exp\left(-\frac{v^2}{2\sigma_c^2}\right) + s_w \exp\left(\frac{-(v-v_w)^2}{2\sigma_w^2}\right) + n_\varepsilon. \tag{2}$$

The ground clutter is modeled by zero mean Doppler velocity, spectrum width σ_c, and maximal power density s_c. The weather signal is modeled by mean velocity v_w, spectrum width σ_w, and maximal power density s_w. The noise component has a constant power density n_ε. To estimate these parameters, this model is fitted to an estimation of the power spectrum (e.g., being estimated with periodogram method) using a standard nonlinear fitting algorithm (e.g., Levenberg–Marquardt method). During the estimation of power spectrum, the limited number of pulses may cause the power leakage from one frequency to other frequencies. Particularly, when clutter power is very strong, its power leakage might overwhelm the weather signal, biasing the estimation of weather spectrum. The application of a window function can greatly reduce the power leakage when power spectrum is estimated, although a window function may broaden the spectrum width somewhat. Considering the tradeoff between sidelobe level and spectrum broadness, STEP applies Blackman–Harris, Blackman, and Hamming windows in accordance with different SNR.

An example of the BGCF is shown in Fig. 2. The green solid line indicates the power spectrum estimated from radar I/Q data. Dashed lines denote the spectrum of clutter and weather components. The blue solid line represents the fitted result, which is the summation of the clutter, weather, and noise components. Although BGCF's result could provide moment estimation of weather signal, the estimation could be further improved in the MLAG module. Considering the real weather spectrum might not follow the Gaussian model assumption in BGCF, the reconstructed spectrum for MLAG processing keeps most of the original spectrum and only removes the clutter portion. Another consideration is that polarimetric radar variables cannot be directly obtained from BGCF. Therefore, moment estimation result in MLAG module, instead of BGCF module, is applied by STEP. The processing of MLAG module requires that the estimated weather spectrum be converted into the time domain. The construction of new I/Q data, which does not contain clutter component, follows (3). First, the Fourier coefficients with amplitude $A(v) = \sqrt{\hat{S}(v)}$ and phase $\varphi(v)$ are calculated with the original I/Q data $s(n)$. Then, the new amplitude $A'(v)$ is obtained after removing the clutter component, whose power spectrum $S_c(v)$ is the fitting result of bi-Gaussian model in (2). The phase $\varphi(v)$ within the clutter range $|v| \le v_c$ has been contaminated by the clutter signal. The contamination would bias the estimation of phase-related radar parameters (e.g., Doppler velocity and differential phase). However, it is difficult to obtain a clean spectrum phase by removing the clutter's contribution from the contaminated phase. It is worth noting that the spectrum phase of a weather signal is statistically uncorrelated in different spectrum bins. Therefore, it is reasonable to use a random phase to replace the phase contaminated by the clutter, as shown in (3d). Although this kind of phase modification might increases the estimation error of phase related parameters, the clutter effect can be mitigated effectively. When the new phase $\varphi'(v)$ is determined, the new Fourier coefficients $F_s'(v)$ are then transformed into new I/Q sequence $s'(n)$ through the inverse fast Fourier transform (IFFT)

$$FFT\left[s(n)\right] = F_s(v) = A(v)e^{j\varphi(v)} \tag{3a}$$
$$F_s'(v) = A'(v)e^{j\varphi'(v)} \tag{3b}$$
$$A'(v) = \sqrt{\hat{S}(v) - S_c(v)} \tag{3c}$$
$$\varphi'(v) = \begin{cases} random, & |v| \le v_c \\ \varphi(v), & |v| > v_c \end{cases} \tag{3d}$$
$$s'(n) = IFFT\left[F_s'(v)\right]. \tag{3e}$$

It is noted that v_c in (3d) represents the boundary of clutter range. That is to say, the clutter contamination is dominant within this range and unimportant beyond. According to the result of bi-Gaussian fitting, the value of v_c is determined when the clutter's power density becomes less than the summation of weather and noise.

There are two issues that might affect the real-time implementation of BGCF. First, the nonlinear regression might have too many iteration cycles before it achieves the convergence. In addition, the regression might not be able to converge if the observed spectrum is not well represented by the bi-Gaussian model. In those cases, BGCF applies a complementary fitting approach with a single-Gaussian weather model to solve the problem. The main difference between implementations of single-Gaussian model and Bi-Gaussian model is whether the spectrum lines within clutter bins are applied for the fitting. As shown in

$$S'(v) = s_w \exp\left(-\frac{(v-v_w)^2}{2\sigma_w^2}\right) + n_\varepsilon \tag{4a}$$

the single-Gaussian fitting method is based on the spectrum model $S'(v)$, which only includes weather and noise components.

The construction of clean I/Q data is similar to the procedure given by (3) except the estimation of new amplitude $A'(v)$, which is given by

$$A'(v) = \begin{cases} \sqrt{S'(v)}, & |v| \le v_c \\ \sqrt{\hat{S}(v)}, & |v| > v_c. \end{cases} \tag{4b}$$

Similar to the GMAP algorithm, the spectrum bins that are contaminated by ground clutter are empirically determined

This article has been accepted for inclusion in a future issue of this journal. Content is final as presented, with the exception of pagination.

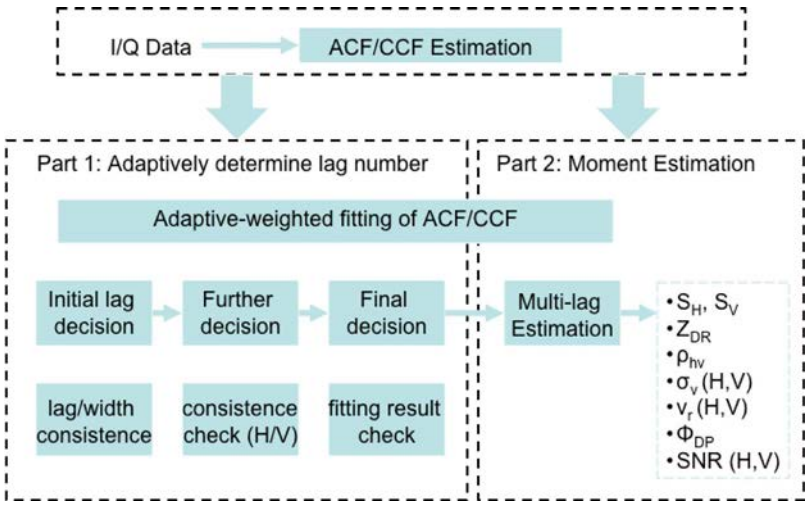

Fig. 3. Flowchart of MLAG algorithm.

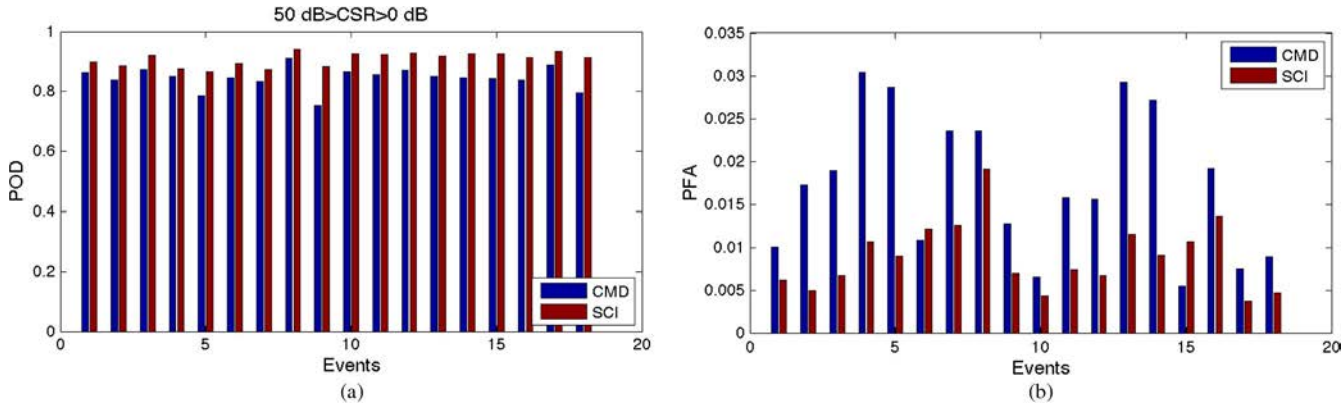

Fig. 4. Comparison of (a) POD and (b) PFA between CMD and SCI algorithms for total 18 experimental data sets.

based on the noise level. A Gaussian curve with a spectrum width of 0.5 m/s is assumed for the clutter spectrum. The amplitude of the Gaussian curve equals the mean power density within the range of ± 0.1 m/s. $v_{\rm c}$ denotes the velocity at which the Gaussian curve arrives at the noise floor in the power spectrum.

D. Multi-Lag Moment Estimator (MLAG)

The concept of multi-lag processing has been described in [10], [12], [13]. Cao *et al.* [14], [15] applied an adaptive weighting to fit ACF and/or CCF of radar signals. The fitted ACF and CCF can then be used to estimate radar variables such as signal power $S_{\rm h}$ (or $S_{\rm v}$), differential reflectivity $Z_{\rm DR}$, correlation coefficient $\rho_{\rm hv}$, spectrum width $\sigma_{\rm h}$ (or $\sigma_{\rm v}$), differential phase $(\Phi_{\rm DP})$ and radial velocity $v_{\rm h}$ (or $v_{\rm v}$). The MLAG module of STEP algorithm is briefly addressed as follows.

As for weather signals, ACF for horizontal polarization $(C_{\rm h})$ and ACF for vertical polarization $(C_{\rm v})$ and CCF $C_{\rm hv}$ are all modeled by a Gaussian function $C_{\rm p}$ (p: h, v, and hv), which is

$$C_p(m) = C_p(0) \exp\left(-\frac{m^2}{2w_p^2}\right) \tag{5}$$

where m is the lag number of ACF/CCF; $w_{\rm p}$ is the decorrelation length of ACF/CCF. The Gaussian ACF/CCF can be fitted through multiple lags of ACF/CCF estimated from I/Q data. The fitting process of MLAG is to minimize the cost function $\chi_{\rm p}$ as

$$\chi_p = \sum_{m=1}^{M} \left[C_p(m) - \left|\hat{C}_p(m)\right|\right]^2 C_p(m). \tag{6}$$

Considering weather signals may decorrelate at farther lags, the cost function in (6) applies an adaptive weighting of the Gaussian model itself. That is, the $C_{\rm p}(m)$, which is to be fitted, serves as a weight in the fitting.

The estimation of radar moments is based on the nonlinear fitting of ACF and CCF (i.e., $C_{\rm h}$, $C_{\rm v}$, and $C_{\rm hv}$). The equations for signal power $S_{\rm h}$ or $S_{\rm v}$, differential reflectivity $Z_{\rm DR}$,

TABLE I
COMPARISON OF POD AND PFA BETWEEN CMD AND SCI ALGORITHMS

	POD (%)					PFA (%)
	CSR (dB) (-20, 50)	(-20, 0)	(-10, 10)	(0, 20)	(0, 50)	
CMD	79.3	27.5	64.8	80.7	84.5	1.73
SCI	88.0	58.5	81.5	89.6	90.8	0.89

This article has been accepted for inclusion in a future issue of this journal. Content is final as presented, with the exception of pagination.

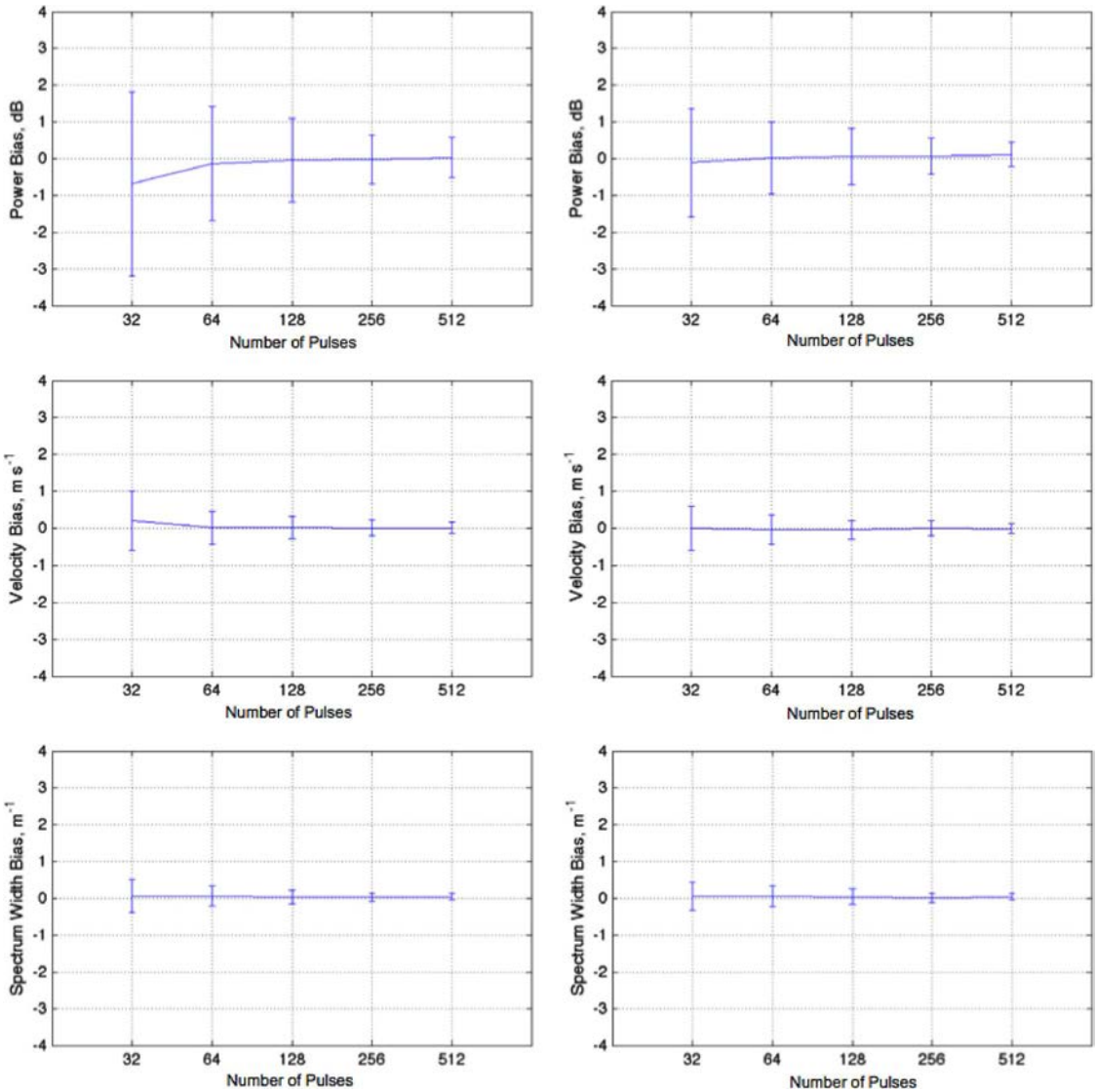

Fig. 5. Effect of the number of pulses on the estimation bias and error of moments processed with BGCF only. Solid lines denote the bias of BGCF processed moments. Vertical bars indicate the standard deviation of estimation error. The three rows from top to bottom show power, velocity, and spectrum width, respectively. Simulated data have CSR $= 10$ dB, and weather spectrum width $\sigma = 2.5$ m/s. The weather velocity is (left column) $v = 2$ m/s, and (right column) $v = 6$ m/s.

correlation coefficient $\rho_{\rm hv}$, and spectrum width $\sigma_{\rm h}$ or $\sigma_{\rm v}$ are given by

$$S_{h,v} = C_{h,v}(0) \tag{7a}$$

$$Z_{DR} = 10\log_{10}\left[\frac{S_h}{S_v}\right](dB) \tag{7b}$$

$$\sigma_{h,v} = \frac{v_a}{\pi w_{h,v}} \tag{7c}$$

$$\rho_{hv} = \frac{C_{hv}(0)}{\sqrt{C_h(0)C_v(0)}} \tag{7d}$$

where $v_{\rm a}$ is the maximum unambiguous velocity. The differential phase $\Phi_{\rm DP}$ and radial velocity $v_{\rm h}$ (or $v_{\rm v}$) are calculated from the weighted average of their estimates on different lags

$$\phi_{DP}(m) = \arg\left[\hat{C}_{hv}(m)\right] - 0.5 \times \left(\arg\left[\hat{C}_h(m)\right] + \arg\left[\hat{C}_v(m)\right]\right) \tag{8a}$$

$$\Phi_{DP} = \frac{\sum_{m=1}^{w_n} C_{hv}(m) \times \phi_{DP}(m)}{\sum_{m=1}^{w_n} C_{hv}(m)} \tag{8b}$$

$$v'_{h,v}(m) = \frac{-v_a}{m\pi} \times \arg\left[\hat{C}_{h,v}(m)\right] \tag{8c}$$

$$v_{h,v} = \frac{\sum_{m=1}^{w_n} C_{hv}(m) \times \text{unwrap}\left[v'_{h,v}(m)\right]}{\sum_{m=1}^{w_n} C_{hv}(m)} \tag{8d}$$

where $w_{\rm n}$ is the integer value of $w_{\rm p}$ and also indicates the number of usable lags; the notation "arg[.]" represents the phase of a complex number; the notation "unwrap[.]" means unwrapping the velocity estimation at different lags $(m > 1)$. Since the velocity aliasing is different for estimations from different lags of ACF, the unwrapping process is needed before averaging.

The flowchart of MLAG is shown in Fig. 3. There are mainly three steps of processing. First, I/Q data are input to estimate the ACF and CCF. Then, the number of usable lags of the ACF/CCF is determined. Third, ACF and CCF at these usable lags are applied to estimate radar moments using (7) and (8). The search of usable lags is the primary issue of multi-lag

This article has been accepted for inclusion in a future issue of this journal. Content is final as presented, with the exception of pagination.

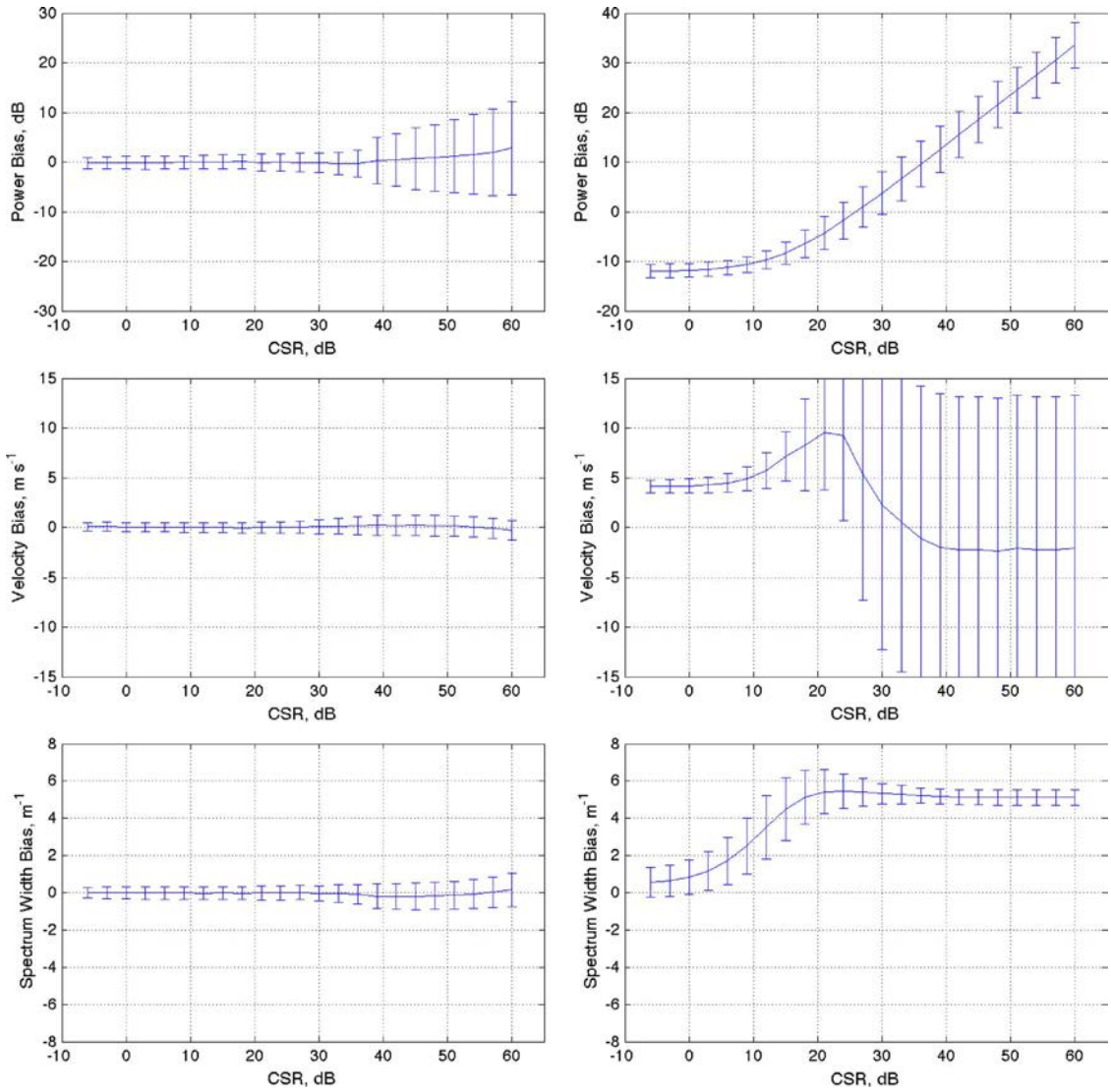

Fig. 6. Effect of CSR on the estimation bias and error of moments. Solid lines denote the bias of moment estimation. Vertical bars indicate the standard deviation of estimation error. The three rows from top to bottom show power, velocity, and spectrum width, respectively. Simulated weather data have a spectrum width $\sigma = 2.5$ m/s, and a velocity $v = 2$ m/s. The number of pulses is 64. The weather velocity is (left column) processing with BGCF, and (right column) processing with -50 dB notch filter (#1) of OU-PRIME.

processing because the more usable lags, the better the multi-lag fitting result. If the ACF/CCF decorrelates faster, there are fewer lags that contain useful weather information. Here, we define the decorrelation length (unit in #) of ACF/CCF as the maximum usable number $w_{\rm n}$. According to equations 6.3 and 6.4 in [8], the relation between $w_{\rm n}$ and spectrum width σ is derived as

$$w_n = \frac{v_a}{\pi\sigma} = \frac{\lambda}{4T_s\pi\sigma} \tag{9}$$

where λ is the radar wavelength and $T_{\rm s}$ is the pulse repetition time. It is seen that the wider the spectrum width, the lower the usable lag number. For example, the C-band OU-PRIME radar normally operates with a pulse repetition frequency of 1180 Hz and its $v_{\rm a}$ is 16.07 m/s. Given that a weather signal has a spectrum width of 0.5–2 m/s, the usable number is 3–10. For S-band radar, if the conditions are the same, the number of usable lags will be double. Consequently, it is expected that the MLAG algorithm would perform better for S-band than for C-band.

There are three criteria to determine the lag number: 1) Is $w_{\rm n}$ consistent with the fitted decorrelation width $w_{\rm p}$, which are estimated from two ACFs (H and V channels) and one CCF, respectively? 2) Are fitted widths for H and V channels, i.e., $w_{\rm h}$, $w_{\rm v}$, and $w_{\rm hv}$, consistent? and 3) Is the fitting error small? These criteria are evaluated iteratively to find the number of lags that gives the best performance. After determining the usable lag, it is straightforward to fit ACF and CCF, and thereby to estimate radar moments using them.

III. Performance of Step Algorithm

A. SCI Performance

The evaluation of clutter identification is based on the simulation of contaminated radar data, which come from OU-PRIME's observations of clear air and storms, in a controlled manner. The clear air data were collected on 08/04/2010 and 01/13/2011. The storm data were collected on 04/12/2009, 10/21/2009, 12/02/2009, 01/21/2010, 04/17/2010, 04/18/2010,

This article has been accepted for inclusion in a future issue of this journal. Content is final as presented, with the exception of pagination.

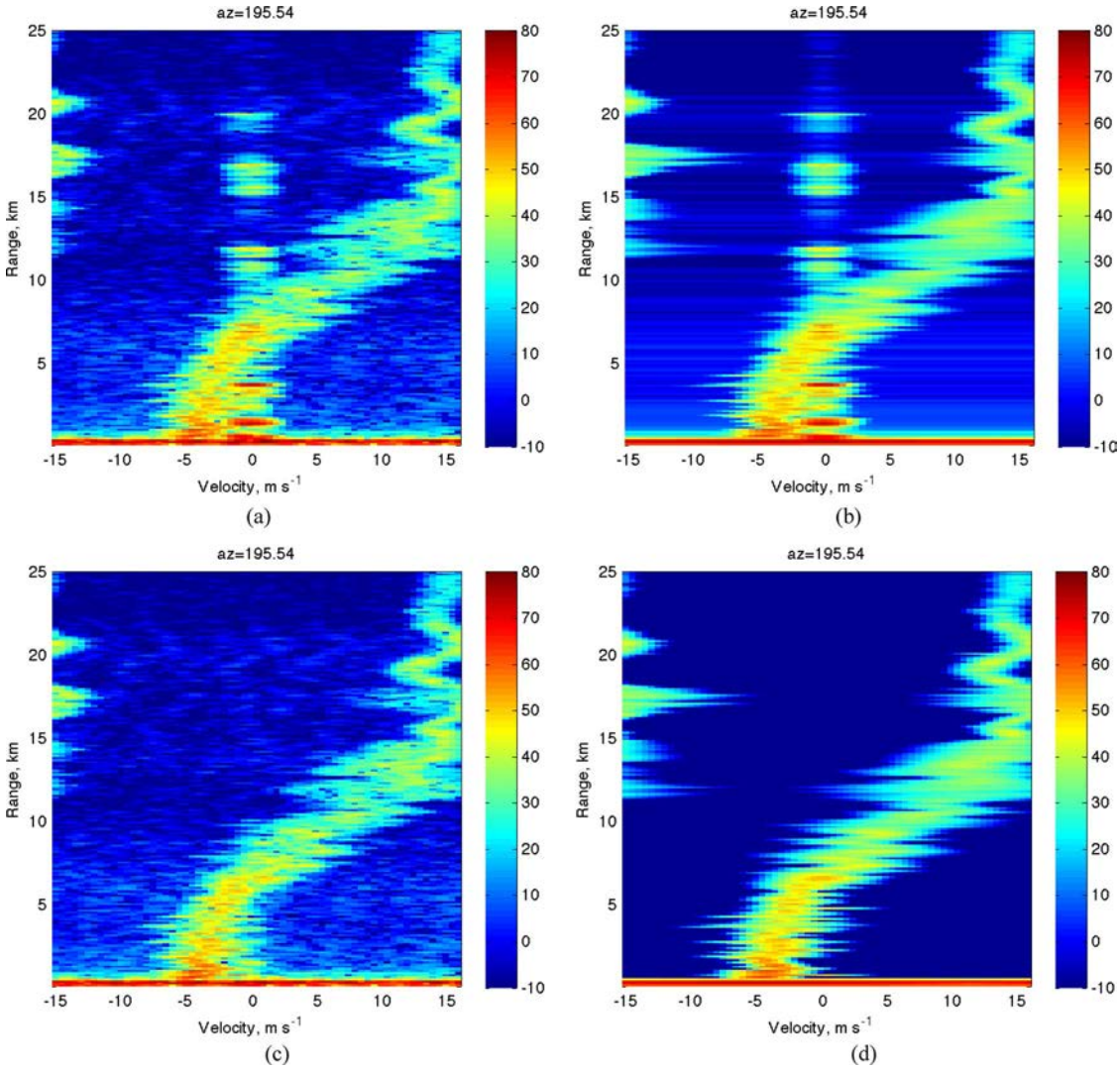

Fig. 7. Range-velocity spectrum example shows BGCF's performance. (a) Contaminated weather spectrum; (b) Bi-Gaussian model result; (c) spectrum of weather only; (d) weather spectrum filtered by BGCF. Weather signals come from OU-PRIME data, 08 September 2010, 2149UTC, 3.5° elevation scan; clutter signals come from OU-PRIME data, 13 January 2011, 2319UTC, 0.45° elevation scan.

05/13/2010, 05/14/2010, and 09/08/2010; these all include widespread stratiform precipitation. The clear air observations at low elevation angles (0° or 0.5°) are assumed to be dominated by ground clutter. The storm observations at higher elevation angle (3.5°) are assumed to be the weather signal without clutter contamination, i.e., the weather truth. The storm data and clear air data (I/Q) are coherently added to simulate the weather data contaminated by clutter. The simulated weather data are then processed with the SCI algorithm. Since the clutter truth and weather truth are known, the quality of the identified result can be quantified through the comparison with the truth. It is worth noting that this approach of simulation will increase the noise level in the combined signal and the estimated weather moment tends to be somewhat worse than assumed weather truth. Moreover, there might still be weak clutter contamination in the 3.5° elevation observations. This kind of contamination is not considered as clutter truth and may result in some false alarms. Regardless of these concerns, the simulation helps to quantitatively assess the SCI algorithm. For comparison, the CMD algorithm is run and evaluated with the same data set.

Fig. 4 shows POD and PFA results of clutter identification using SCI and CMD algorithms. The clutter truth for cases 1–9 comes from clear air observation at 0.5° while the remaining cases use observations at 0°. The PFA is calculated using pixels without clutter contamination, i.e., the region outside of clutter mask. According to the processing of experimental data, Fig. 4 shows SCI generally has higher detection rate and lower false alarm rate than CMD algorithm, which has been widely recognized as a sufficient clutter identifier for operational use in the NEXRAD network. The mean POD and PFA of all these cases are summarized in Table I. For low CSR, e.g., $0\ \text{dB} > \text{CSR} > -20\ \text{dB}$, SCI is much better than CMD. For $\text{CSR} > 0$ dB, SCI has POD over 90%, which is about 6 percentage points more than CMD. On average, SCI has a low PFA, around 0.9% and lower than CMD's 1.73%.

B. BGCF Performance

The performance of BGCF depends on the number of pulses used to estimate the power spectrum. Fig. 5 shows the trend of

This article has been accepted for inclusion in a future issue of this journal. Content is final as presented, with the exception of pagination.

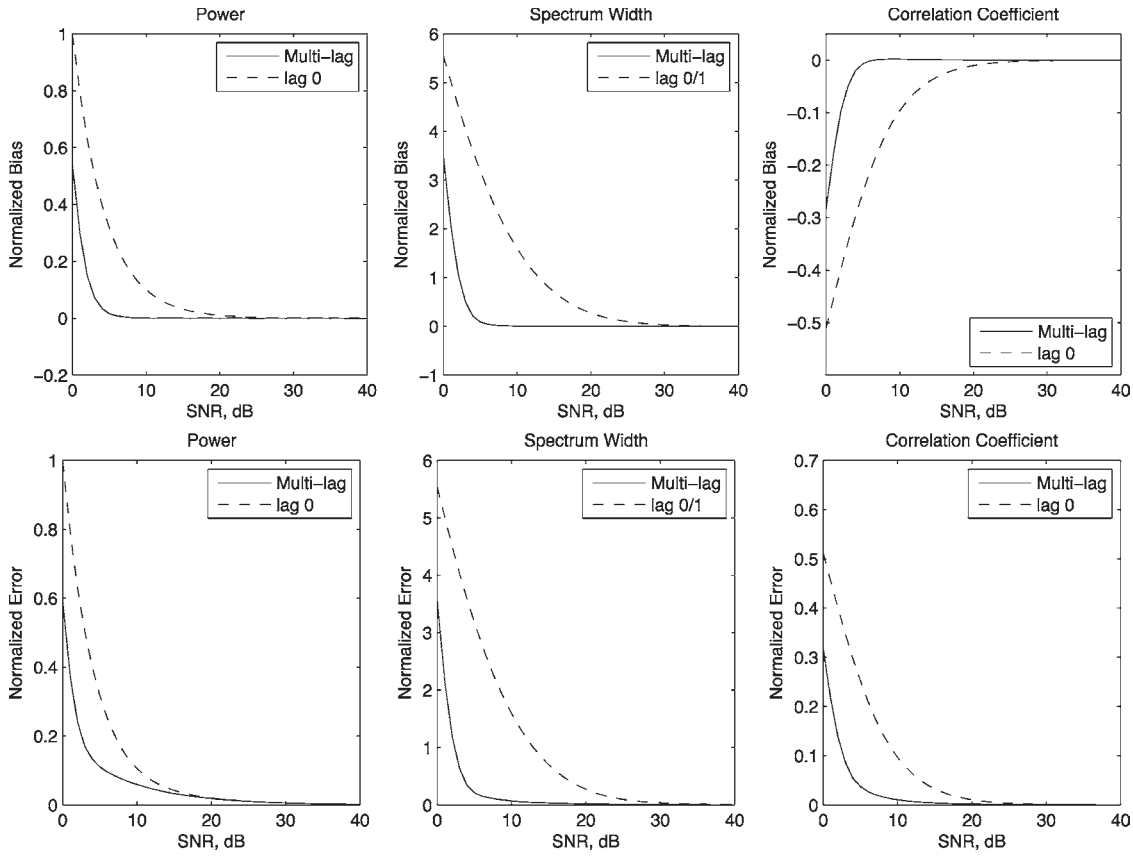

Fig. 8. Quantification of moment estimation by MLAG method. (a) Power; (b) spectrum width; and (c) correlation coefficient. The upper row shows the normalized estimation bias and the lower row shows the normalized estimation error. The number of pulses of the weather signal is 38.

this dependence. As Fig. 5 shows, the BGCF performance is improved with increasing the number of pulses. This is reasonable because more data points in the power spectrum can lead to an improved fitting. In addition, the right column shows a better performance than the left column. This fact implies that fitting a spectrum with weather and clutter components separated out is easier than fitting an overlapped spectrum. It is worth noting that BGCF based on 64 pulses generally performs well. BGCF based on 32 pulses can also function well if the weather and clutter signals are well separated in the spectral domain.

The performance of BGCF also depends on the CSR. Fig. 6 shows its quantification and compares BGCF results with the results of the notch filter that is embedded in the signal processor of OU-PRIME, which has a clutter suppression of -50 dB. As Fig. 6 shows, BGCF method demonstrates a superb performance in removing the clutter contamination (much better than traditional notch filter method). The power, velocity, and spectrum width estimates have very small biases, particularly for CSR < 30 dB. The estimation errors are also minor. For example, as for CSR < 30 dB, the errors of power, velocity, and spectrum width estimations are within 2 dB, 0.7 m/s, and 0.4 m/s, respectively. The notch filter, however, causes a large bias for all three moments. The bias and error of BGCF are insignificant for small to moderate CSRs. When CSR is large, e.g., CSR > 35 dB, BGCF's performance tends to degrade, but still not much. Even for CSR $= 60$ dB, the power bias is only around 3 dB although the standard error increases to 9 dB. Fig. 6 also implies that the increase of CSR has little effect on the estimation of velocity and spectrum width.

Fig. 7 gives an example of range-velocity spectrum to illustrate BGCF's performance. Fig. 7(a) shows the contaminated weather spectrum. This range-velocity spectrum is calculated from combined weather and clutter signals. Weather signals come from the 3.5° elevation scan of storm observed by OU-PRIME on 08 September 2010 and clutter signals come from the 0.45° elevation scan of clear air on 13 January 2011. Fig. 7(c) shows the weather spectrum only, denoting the weather truth. Using BGCF processing, weather, clutter, and noise components are estimated. Their combined spectrum is shown in Fig. 7(b), and the filtered weather spectrum is shown in Fig. 7(d). The performance of BGCF algorithm is well demonstrated through the comparison of Fig. 7(a) and (b) as well as the comparison of Fig. 7(c) and (d). It is shown in the range-velocity spectrum that the weather signal filtered by BGCF matches the weather truth very well.

C. MLAG Performance

The MLAG method can improve moment estimation in the presence of noise. Based on simulated weather signals, Lei *et al.* [13] have given detailed analysis of MLAG's performance for some fixed lags. The most effective improvements are achieved in estimating power, spectrum width, and correlation coefficient. Using real weather observation, Fig. 8 shows quantification of MLAG method for these three moments. The data used for this analysis come from weather observations using OU-PRIME and simulated random noise. The observed weather signal with SNR$>$40 dB is assumed to be weather

This article has been accepted for inclusion in a future issue of this journal. Content is final as presented, with the exception of pagination.

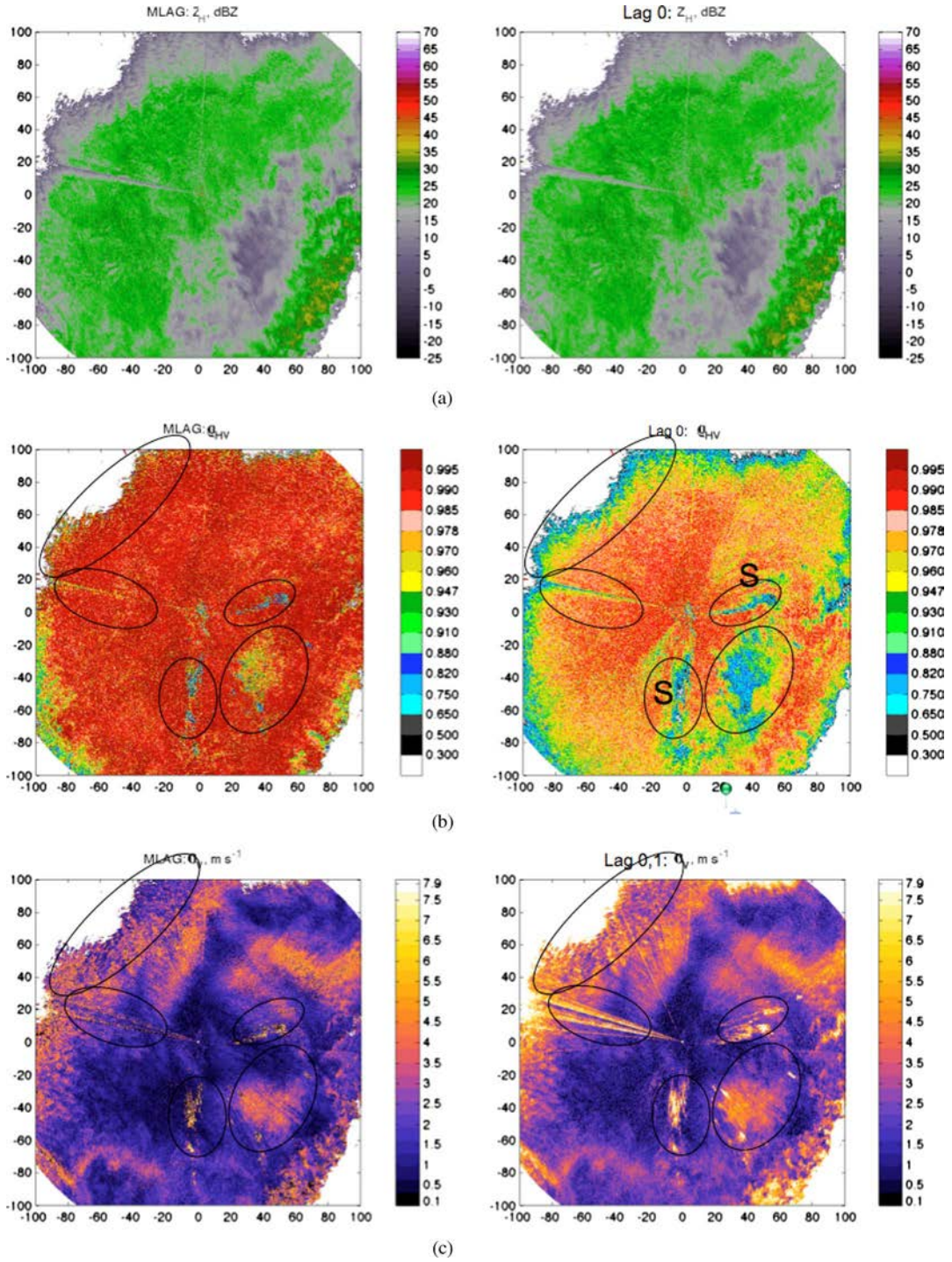

Fig. 9. Comparison of MLAG result and conventional moment estimation. (a) Reflectivity; (b) correlation coefficient; and (c) spectrum width. OU-PRIME data are collected on 15 June 2010, 0601UTC, $El = 0.5°$. Mark "S" points out regions that are contaminated by the second trip echo.

truth without noise. The random noise is added to the weather truth in order to simulate weather signals with different levels of SNR. The estimation bias and error, which are normalized by the weather truth, are then calculated from the result of MLAG processing.

As Fig. 8 shows, moment estimation with a lower SNR normally has a higher estimation bias (or error). The trends of estimation bias and estimation error generally follow each other. The MLAG method can effectively improve power, spectrum width, and correlation coefficient estimation for SNR < 20 dB. The improvement is more evident for low SNRs (i.e., SNR $<$ 5 dB). It should be noted that the real weather signals might not be well modeled by Gaussian ACF/CCF, and therefore could introduce model errors during the multi-lag fitting. Since Fig. 8 applies the real weather data, the results include this effect. In addition to the mitigation of noise effects, another advantage of MLAG method is that it can mitigate the contamination of second trip echoes for radars utilizing a magnetron transmitter, which inherently has random phase coding [15]. The details of the second trip mitigation are not presented here.

This article has been accepted for inclusion in a future issue of this journal. Content is final as presented, with the exception of pagination.

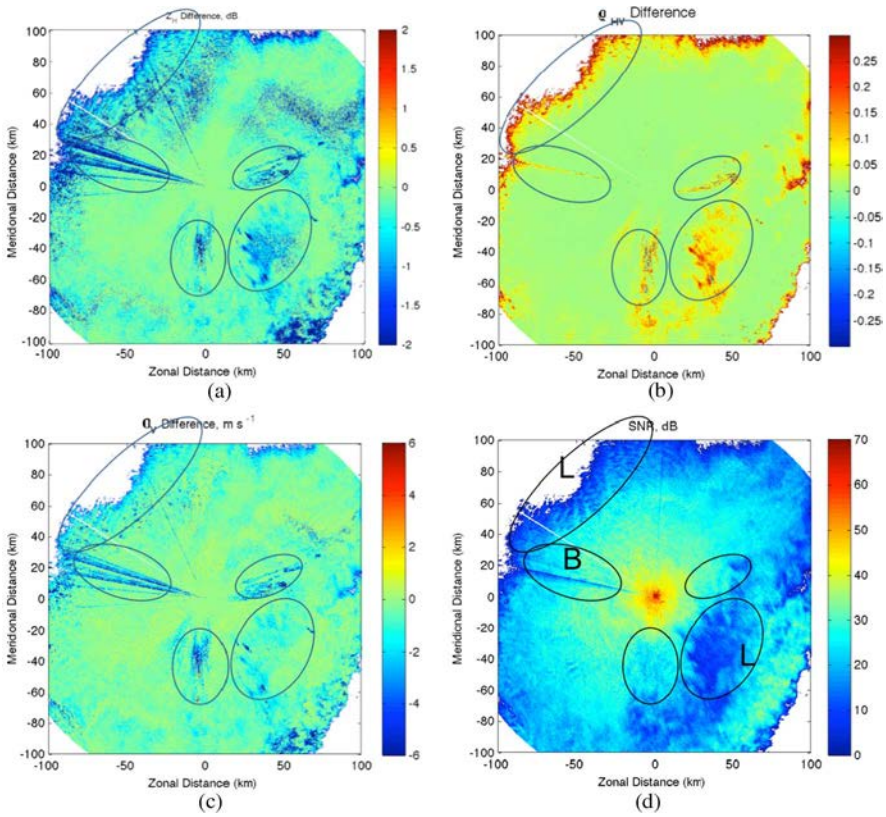

Fig. 10. Supplementary figures for comparison in Fig. 9. (a) Reflectivity difference; (b) correlation coefficient difference; (c) spectrum width difference; and (d) SNR. The estimation difference is calculated by MLAG results subtracting conventional estimation results. Mark "L" denotes example region with a low SNR. Mark "B" indicates example region suffering from a partial beam blockage with reduced SNRs.

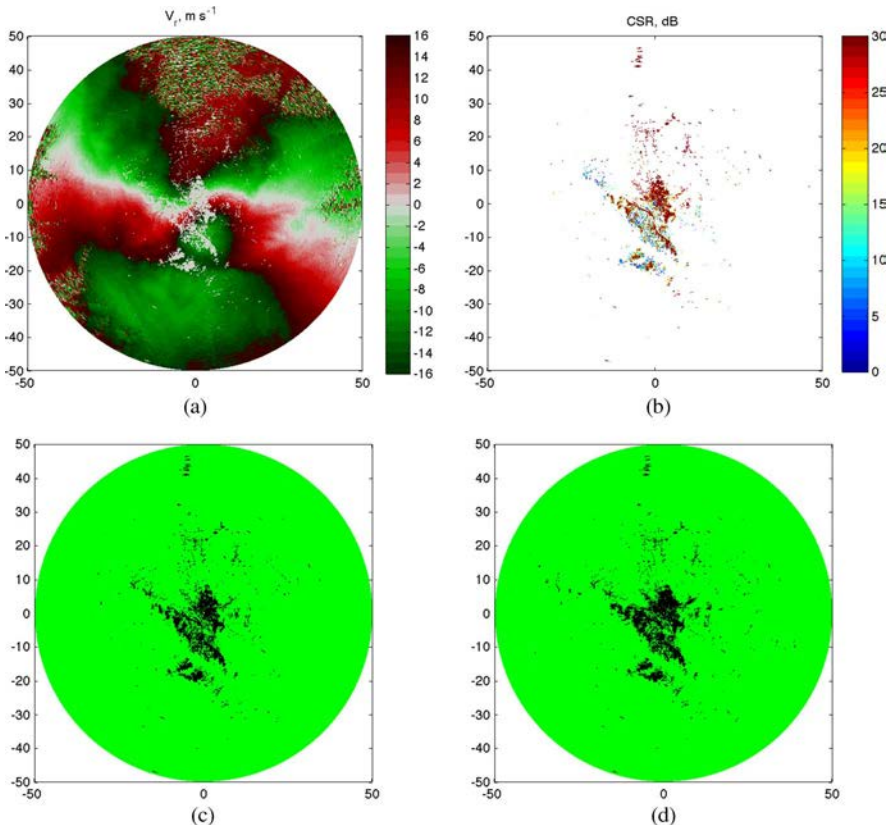

Fig. 11. Example of STEP processing (clutter identification). (a) Radial velocity; (b) CSR; (c) clutter truth; (d) STEP identified clutter pixels (POD $= 97.5\%$, PFA $= 2.6\%$). Weather signals come from OU-PRIME data, 21 October 2009, 1803UTC, 3.5° elevation; clutter signals come from OU-PRIME data, 13 January 2011, 2319UTC, 0.05° elevation angle.

This article has been accepted for inclusion in a future issue of this journal. Content is final as presented, with the exception of pagination.

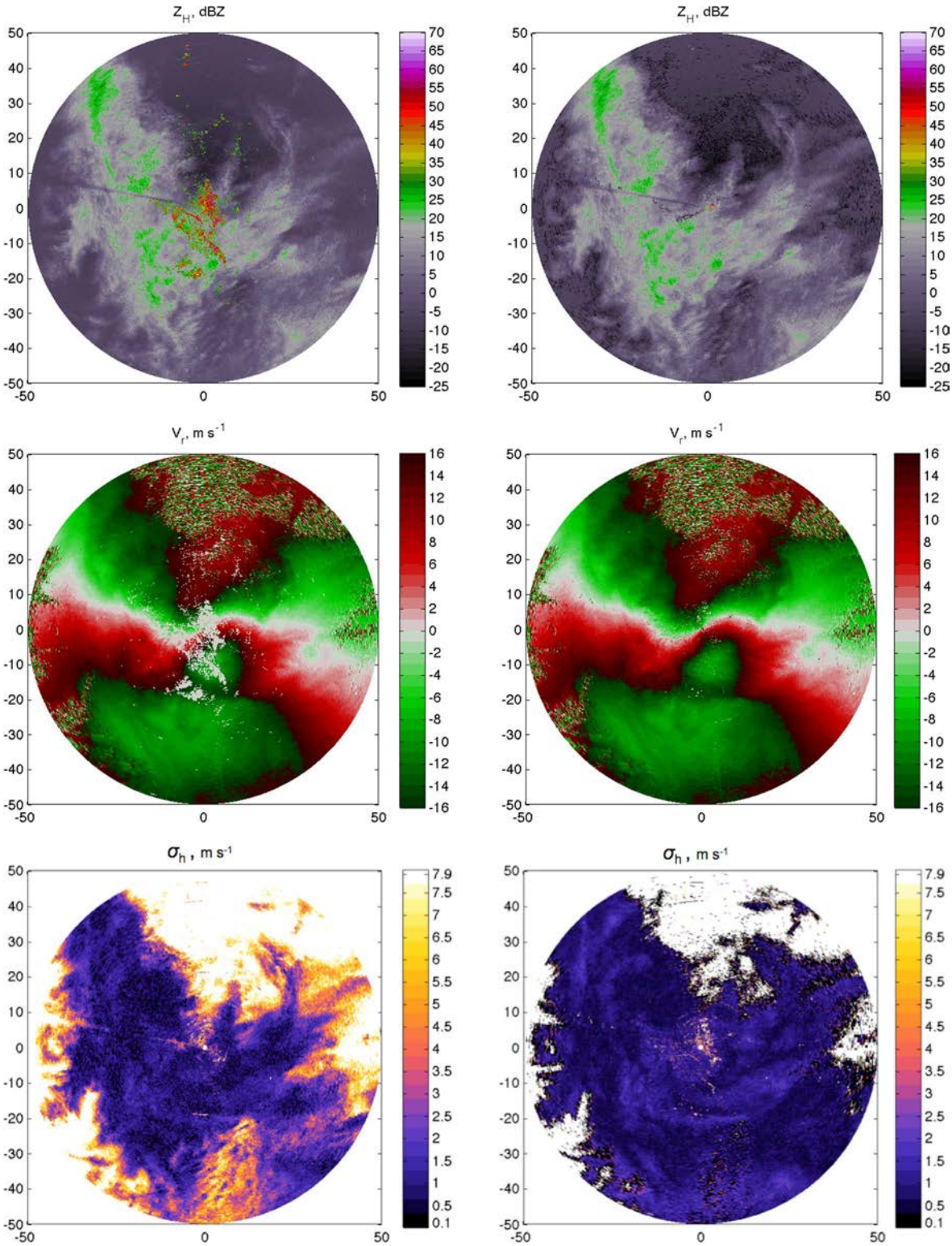

Fig. 12. Comparison of (left column) contaminated moments and (right column) STEP processed moments. Six rows show radar reflectivity Z_{H}, radial velocity v_{h}, spectrum width σ_{h}, correlation coefficient ρ_{hv}, differential phase Φ_{DP}, and differential reflectivity Z_{DR}, respectively (the same data as Fig. 11).

Figs. 9 and 10 show an example of MLAG processing. The precipitation observed by OU-PRIME on 15 June 2010 generally includes widespread moderate or light rain. The left panels in Fig. 9 denote the MLAG processing result and right figures are conventional estimates based on lag zero (and one) of ACF/CCF. To explain the comparison better, Fig. 10 provides images of moment difference between MLAG result and conventional result. The SNR of radar measurement is also presented in Fig. 10(d), which shows a large region of measurement has a SNR less than 20 dB. Mark "L" denotes the region with a low SNR. Mark "B" indicates the region suffering from a partial beam blockage with reduced SNRs. As shown

This article has been accepted for inclusion in a future issue of this journal. Content is final as presented, with the exception of pagination.

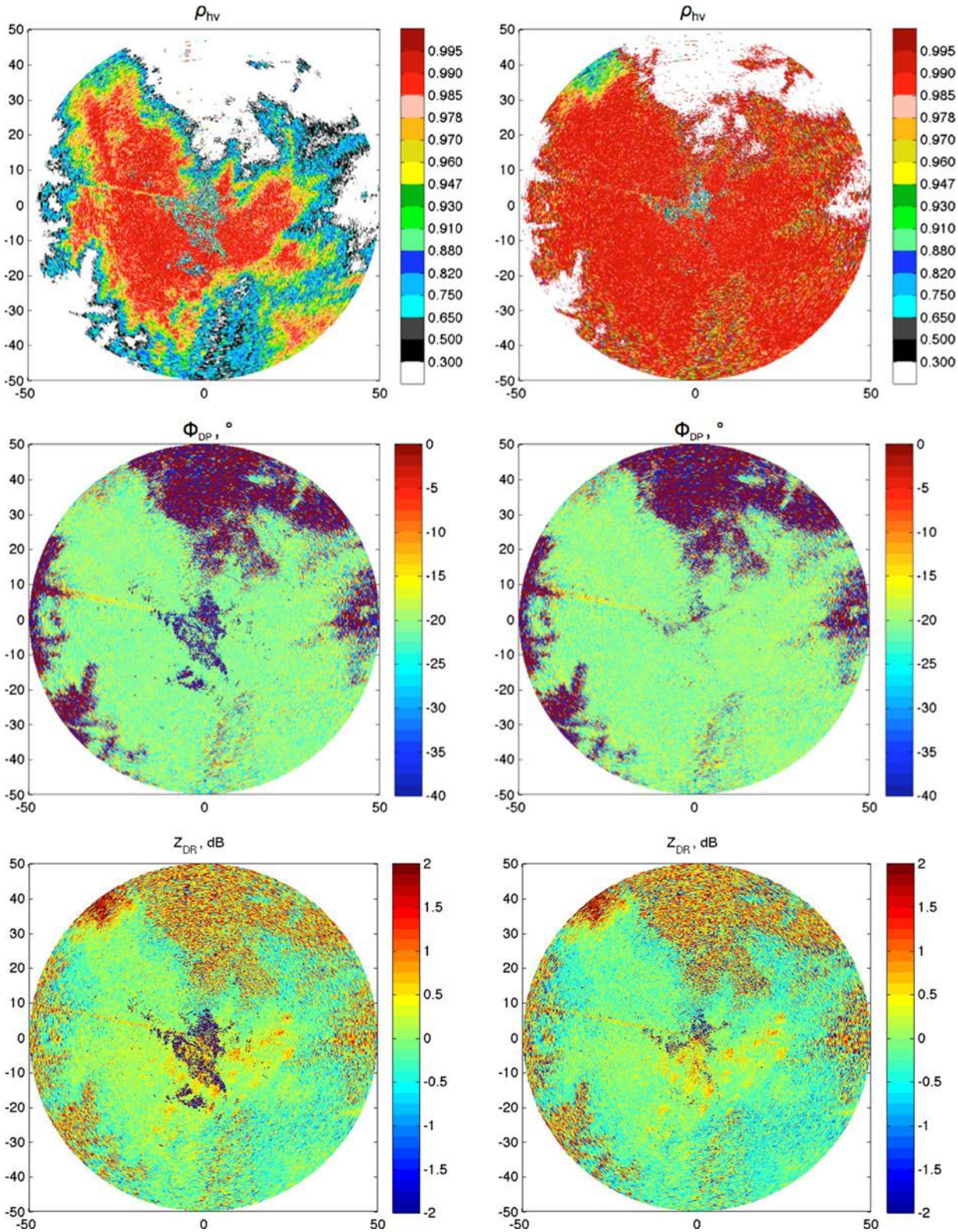

Fig. 12. *(Continued).* Comparison of contaminated moments (left column) and STEP processed moments (right column). Six rows show radar reflectivity Z_{H}, radial velocity v_{h}, spectrum width σ_{h}, correlation coefficient ρ_{hv}, differential phase Φ_{DP}, and differential reflectivity Z_{DR}, respectively (the same data as Fig. 11).

in the right panel of Fig. 9(b), mark "S" points out regions that are contaminated by the second trip echo. According to conventional lag zero estimator, ρ_{hv} values at L, B, and S regions are obviously underestimated. It is clearly shown in Fig. 10 that MLAG improves the moment estimation. Reflectivity and spectrum width values at L, B, and S regions are reduced and ρ_{hv} are enlarged after the processing by MLAG. The whole precipitation region generally has a high ρ_{hv} value

This article has been accepted for inclusion in a future issue of this journal. Content is final as presented, with the exception of pagination.

close to 1, implying the radar measurement is precipitation echo.

IV. Case Study of Step Algorithm

The STEP algorithm has a complete combination of aforementioned advantages from its three modules. The rest of this section gives a real data example to demonstrate the superior performance of STEP.

Fig. 11 shows a case from 21 October 2009, whose data are combined with the clutter observation on 13 January 2011. Fig. 11(b) shows the plan position indicator image of CSR. In the image, the pixel with CSR > 0 dB is assumed to have clutter contamination. Accordingly, the image of clutter truth is shown in Fig. 11(c). Fig. 11(a) shows the velocity estimation based on the traditional lag one estimation. It is seen that the clutter-contaminated pixels are biased toward 0 m/s. Fig. 11(d) shows the clutter identification result, which has been processed with the STEP algorithm. Comparing the STEP result with the clutter truth, we see that the feature of the clutter region is quite similar for both images. Further comparison shows that the POD of STEP is 97.5% and the PFA is 2.6%.

Fig. 12 compares the original moments of contamination (shown in the left column) with the results processed by STEP (shown in the right column). Six rows of figures, from top to bottom, give the results of radar reflectivity $Z_{\rm H}$, radial velocity $v_{\rm h}$, spectrum width $\sigma_{\rm h}$, correlation coefficient $\rho_{\rm hv}$, differential phase $\Phi_{\rm DP}$, and differential reflectivity $Z_{\rm DR}$, respectively. For radar reflectivity, the clutter contamination is evident in the original result with a very high value while it is gone in the STEP result. There is only a small area where it is overfiltered by STEP. The storm in this area has a near-zero radial velocity and narrow spectrum width. For radial velocity, biases are clearly seen in the original result while they disappear in the STEP result, which gives a smooth velocity field in the clutter region. For spectrum width, the original result shows larger values in the region of low SNR and smaller values in the clutter region. The STEP result reduces the estimation for the low SNR region and increases the estimation for the clutter region. The improved spectrum width image looks more smooth and consistent within the storm region. For correlation coefficient, lower values are shown for both clutter and low SNR regions in the original result. The values for these two regions have been increased in the STEP result, indicating that precipitation is present in these regions. Now, the image of correlation coefficient is smooth enough that the radar echo can be easily classified as precipitation. For differential phase and differential reflectivity, the clutter contamination is clearly shown in the original results. The STEP results give a much cleaner image for both moments. The recovered moments in contaminated region are generally consistent with those results in uncontaminated region. An interesting region is the northwest corner where the STEP result does not show much change. Considering the data set is for observations at 3.5° elevation, radar echo in that region (at the range of about 50 km) might partially come from melting particles. As we know, the mixing phase of raindrops and melting snow/ice particles may lead to the reduction of correlation coefficient, the increase of differential reflectivity, and the large variation of differential phase, which can all be seen in Fig. 12. Therefore, the northwest corner region is likely attributed to the observation of melting particles and not to the noise effect. It makes sense that the STEP result is consistent with the conventional result there. From the example shown in Fig. 12, it is well demonstrated that the STEP algorithm can extensively improve the moment estimation for the application of polarimetric weather radar.

V. Conclusion

STEP is an advanced signal-processing framework that takes advantage of latest advances in clutter identification, filtering, and moment estimation. The major feature of STEP algorithm is that it combines signal processing in both time and spectral domains, making it effective in mitigating clutter and noise effects on radar moment estimation. It is worth noting that STEP's performance improves with increasing numbers of pulses. The STEP algorithm has been extensively tested with OU-PRIME data sets using 0.5 or 1° angular resolution and shows good performance in improving the quality of polarimetric radar data.

Compared to popular clutter filtering or moment estimation algorithms (e.g., CMD, GMAP, lag one estimator), the STEP algorithm adopts a more complex scheme and, therefore, requires more computational resources. This is a concern for the real-time implementation. As a result, further optimization and simplification work is on going. This work will be evaluated using EEC's operational IQ2(TM) signal processor and tested with OU-PRIME.

Acknowledgment

The authors are grateful to ARRC's research scientists and radar engineers in maintaining OU-PRIME radar and collecting radar data.

References

[1] S. M. Torres and D. S. Zrnic, "Ground clutter canceling with a regression filter," *J. Atmos. Ocean. Technol.*, vol. 16, no. 10, pp. 1364–1372, Oct. 1999.

[2] A. D. Siggia and R. E. Passarelli, "Gaussian model adaptive processing (GMAP) for improved ground clutter cancellation and moment calculation," in *Proc. 3rd Eur. Conf. Radar Meteorol. Hydrol.*, Visby, Sweden, 2004, pp. 67–73.

[3] K. D. Le, R. D. Palmer, B. L. Cheong, T.-Y. Yu, G. Zhang, and S. M. Torres, "On the use of auxiliary receive channels for clutter mitigation with phased array weather radars," *IEEE Trans. Geosci. Remote Sens.*, vol. 47, no. 1, pp. 272–284, Jan. 2009.

[4] J. C. Hubbert, M. Dixon, and S. M. Ellis, "Weather radar ground clutter. Part II: Real-time identification and filtering," *J. Atmos. Ocean. Technol.*, vol. 26, no. 7, pp. 1181–1197, 2009.

[5] D. Warde and S. Torres, "A novel ground-clutter-contamination mitigation solution for the NEXRAD network: The CLEAN-AP filter. Preprints," presented at the 26th Int. Conf. IIPS Meteorology, Oceanography, Hydrology—Amer. Meteor. Soc., Atlanta, GA, 2010, 2010, paper 8.6, 2010.

[6] D. N. Moisseev and V. Chandrasekar, "Polarimetric spectral filter for adaptive clutter and noise suppression," *J. Atmos. Oceanic Technol.*, vol. 26, no. 2, pp. 215–228, Feb. 2009.

[7] Y. Li, G. Zhang, and R. Doviak, "A new approach to detect the ground clutter mixed with weather echoes," in *Proc. IEEE RADAR*, May 23–27, 2011, pp. 622–626, 2011.

[8] R. J. Doviak and D. S. Zrnić, *Doppler Radar and Weather Observations*. New York: Academic, 1993.

[9] V. M. Melnikov and D. S. Zrnić, "Autocorrelation and cross-correlation estimators of polarimetric variables," *J. Atmos. Ocean. Technol.*, vol. 24, no. 8, pp. 1337–1350, Aug. 2007.

[10] G. Zhang, R. Doviak, J. Vivekanandan, W. Brown, and S. A. Cohn, "Performance of correlation estimators for spaced antenna wind measurement

This article has been accepted for inclusion in a future issue of this journal. Content is final as presented, with the exception of pagination.

in the presence of noise," *Radio Sci.*, vol. 39, no. 3, p. RS3017, 2004. doi:10.29/2003RS003022.
[11] M. Pinsky, J. Figueras i Ventura, T. Otto, A. Sterkin, A. Khain, and H. W. J. Russchenberg, "Application of a simple adaptive estimator for an atmospheric Doppler radar," *IEEE Trans. Geosci. Remote Sens.*, vol. 49, no. 1, pp. 115–127, Jan. 2011.
[12] L. Lei, G. Zhang, R. D. Palmer, B. L. Cheong, and M. Xue, "A multi-lag correlation estimator for polarimetric radar variables in the presence of noise," in *Proc. 34th Conf. Radar Meteorol.*, Williamsburg, VA, Oct. 5–9, 2009.
[13] L. Lei, G. Zhang, R. Doviak, R. Palmer, B. Cheong, M. Xue, Q. Cao, and Y. Li, "Multi-lag correlation estimators for polarimetric radar measurements in the presence of noise," *J. Atmos. Ocean. Technol.*, to be published.
[14] Q. Cao, G. Zhang, and R. Palmer, "Real-time implementation of enhanced moment estimation on the C-band polarimetric research radar OU-PRIME," in *Proc. ERAD*, Sibiu, Romania, Sep. 6–10, 2010.
[15] Q. Cao, G. Zhang, R. D. Palmer, and L. Lei, "Detection and mitigation of second trip echo in polarimetric weather radar employing random phase coding," *IEEE Trans. Geosci. Remote Sens.*, vol. 50, no. 4, pp. 1240–1253, Apr. 2012.
[16] R. Palmer, D. Bodine, M. Kumjian, B. Cheong, G. Zhang, Q. Cao, H. B. Bluestein, A. Ryzhkov, T.-Y. Yu, and Y. Wang, "Observations of the 10 May 2010 tornado outbreak in central oklahoma using OU-PRIME: Potential for new science with high-resolution polarimetric radar," *Bull. Amer. Meteorol. Soc.*, vol. 92, pp. 871–891, 2011.
[17] M. A. Rico-Ramirez and I. D. Cluckie, "Classification of ground clutter and anomalous propagation using dual-polarization weather radar," *IEEE Trans. Geosci. Remote Sens.*, vol. 46, no. 7, pp. 1892–1904, Jul. 2008.
[18] H. S. Park, A. V. Ryzhkov, D. S. Zrnić, and K. Kim, "The hydrometeor classification algorithm for the polarimetric WSR-88D: Description and application to an MCS," *Weather Forecast.*, vol. 24, no. 3, pp. 730–748, Jun. 2009.
[19] C. M. Nguyen, D. N. Moisseev, and V. Chandrasekar, "A parametric time domain method for spectral moment estimation and clutter mitigation for weather radars," *J. Atmos. Ocean. Technol.*, vol. 25, no. 1, pp. 83–92, Jan. 2008.

Qing Cao (M'07) received the B.S. and M.S. degrees in electrical engineering from Wuhan University, Wuhan, China, in 1997 and 2005, respectively, and the Ph.D. degree in electrical engineering from the University of Oklahoma (OU), Norman, in 2009.

He was a Telecom Engineer in China from 1997 to 2002, working on wireless communication systems. From 2002 to 2005, he was with the Radio Wave Propagation Laboratory, Wuhan University, performing research on high-frequency ground wave radar systems. Since 2006, he has been with the Atmospheric Radar Research Center, OU, where he was first a Graduate Assistant, then a Postdoctoral Researcher, and currently a Research Associate. His research interests include remote sensing techniques, radar signal processing, and radar polarimetry for precipitation estimation and forecast.

Dr. Cao has been a member of the American Meteorological Society since 2007.

Guifu Zhang (S'97–M'98–SM'02) received the B.S. degree in physics from Anhui University, Hefei, China, in 1982, the M.S. degree in radio physics from Wuhan University, Wuhan, China, in 1985, and the Ph.D. degree in electrical engineering from the University of Washington, Seattle, in 1988.

From 1985 to 1993, he was an Assistant and Associate Professor with the Space Physics Department, Wuhan University. In 1989, he was a Visiting Scholar at the Communications Research Laboratory, Japan. From 1993 to 1998, he studied and worked in the Department of Electrical Engineering, University of Washington, Seattle, where he was first a Visiting Scientist and later a Ph.D. student. He was a Scientist with the National Center for Atmospheric Research. He joined the School of Meteorology, University of Oklahoma, Norman, in 2005. His research interests include modeling of wave propagation and scattering in geophysical media and the development of remote sensing techniques for monitoring the Earth environment and understanding physical processes. He is currently interested in radar polarimetry and interferometry for weather quantification and forecasting.

Robert D. Palmer was born in Fort Benning, GA, on June 3, 1962. He received the Ph.D. degree in electrical engineering from the University of Oklahoma (OU), Norman, in 1989.

From 1989 to 1991, he was a Japan Society for the Promotion of Science Postdoctoral Fellow with the Radio Atmospheric Science Center, Kyoto University, Kyoto, Japan, where his major accomplishments were the development of novel interferometric radar techniques for studies of the lower and middle atmospheres. From 1993 to 2004, he was a memberof the faculty of the Department of Electrical Engineering, University of Nebraska, Lincoln, where his interests broadened into areas including wireless communications, remote sensing, and pedagogy. He is currently the Tommy C. Craighead Chair of the School of Meteorology, OU, where he is also an Adjunct Professor with the School of Electrical and Computer Engineering. He serves as Director of OU's interdisciplinary Atmospheric Radar Research Center, which is the focal point for the weather radar research and educational activities on the Norman campus. Since he came to OU, his research interests have been focused primarily on the application of advanced radar signal processing techniques to observations of severe weather, particularly related to phased array radars and other innovative system designs. He has published widely in the area of radar remote sensing of the atmosphere, with emphasis on generalized imaging problems, spatial filter design, and clutter mitigation using advanced array/signal processing techniques.

Dr. Palmer is a member of URSI Commission F, the American Geophysical Union, and the American Meteorological Society. He has been the recipient of several awards for both his teaching and research accomplishments.

Michael Knight spent 33 years in research and development of weather radar systems and related components. Currently, he is serving as the Vice President of Engineering for Enterprise Electronics Corporation, Enterprise, AL.

Ryan May received the B.S. and M.S. degrees in meteorology from The University of Oklahoma, Norman, OK, in 2003 and 2005, respectively. He is currently working toward the Ph.D. degree in meteorology in the School of Meteorology, University of Oklahoma, Norman.

His research interests include data visualization and adaptive weather radar algorithms and signal processing. Since 2009, he has been a Software Engineer at Enterprise Electronics Corporation, Enterprise, AL, working on dual polarimetric algorithms and adaptive signal processing for the Enterprise Doppler Graphics Environment.

Robert J. Stafford received the B.Sc. degree in computing and information systems from The University of Manchester, Manchester, U.K., in 1987.

Since then, he has been working in the commercial radar business with Plessey Radar/Siemens Plessey Systems (Isle of Wight, U.K.), Lassen Reseach (Chico, CA) and the last 15 years with Enterprise Electronics Corporation, Enterprise, AL. His primary focus and responsibility have been in software for radar control and data processing systems.